Silicon (2022) 14:977–987
https://doi.org/10.1007/s12633-020-00874-8

Influence of Si Content on Fatigue Life for Heat Treated Cast Al-Si-mg Alloy Using Different Quenching Technique

S. Ramesh Kumar[1] · M. SreeArravind[1]

Received: 29 September 2020 / Accepted: 30 November 2020 / Published online: 6 January 2021

Abstract
Al-Si-Mg aluminum alloy samples were subjected to solution heat treatment at the temperature of 520 °C for 2 h to attain T42 condition. The heat-treated samples were quenched further in air and water mediums. After quenching, the fatigue life was analyzed with the total strain amplitude (TSA) of 0.4% at the cyclic frequency of 0.3 Hz using a low cycle fatigue testing machine. Air quenched sample has higher life with 1286 cycles than heat-treated and water quenched sample, which were having a fatigue life of 836 cycles and 708 cycles. Tensile mean stress was observed in all samples due to residual stress. Due to fatigue striation, ripple formation was observed in the air quenched sample, and the ripple having the size of 2-3 μm observed under SEM fractography. XRD peaks of Mg_2Si and Al_3Fe precipitates confirm the proper dispersion during the solution heat treatment.

Keywords Aluminum alloy · Al-Si-mg · SEM · XRD · Strain controlled fatigue · Heat treatment. Stress-strain curve

1 Introduction

Al-Si-Mg aluminum alloy (AA6063) has been utilized widely in the structural part in the aerospace and automotive industries. Due to the application circumstance, the material undergoes cyclic deformation, which leads to early failure. The solution heat treatment of aluminum alloy was done to obtain optimal mechanical properties. The main objective of heat treatment is to maximize the effect of precipitates in the alloy [1, 2]. The final property of the materials depends on the post-heat treatment process, such as quenching. The rate of cooling decides the fine dispersion of the precipitates and control the distortion. So the optimal cooling rate is required to achieve the desired mechanical properties [3]. Ridhwan et al. observed an increase in hardness and tensile strength after the solution heat treatment of Al 6061 at 530 °C, the formation of precipitate Mg_2Si provides heat treatability to the aluminum 6xxx alloys [4]. Hamzah et al. defined that the rate of cooling and quenching medium influences the microstructure and hardness [5]. Roselita et al. concluded that heat treatment of the spring steel showed a positive effect on fatigue life, thereby inducing the compressive residual stresses of the steel [6]. Nasir et al. found 7.2% difference in fatigue life among the heat treated and, as received aluminum 6061 alloys [7]. In aluminum alloy 6061, the solution heat treatment followed by the precipitation heat treatment influenced the fatigue life of the sample and the increase in the hardness value [8]. Heat treatment of aluminum alloy influences the grain size and precipitation structure. Since there is a complex interaction between the loading and microstructure, the fatigue life of aluminum alloys got influenced by the above factors [9].Frodal et al. reported that quenching medium influences the crack initiation, and air cooled samples experienced slow crack propagation compared to water quenching [10]. They also investigated the material behavior in plasticity by using the nanostructure model and found an interaction between hard precipitate strengthened regions and precipitate free zones. Liu et al. found slow cooling of aluminum alloy 7085 leads to higher hardness, and quenching induced the tensile strength [11]. Additionally, the air cooled aluminum sample exhibit better mechanical properties than the water quenched sample.

Kwofie et al. stated that an increase in mean tensile stress during the low cycle fatigue might increase the fatigue life of soft materials up to specific cycles and propose a stress life strategy to correlate the low cycle fatigue life of a sample under mean stress [12]. Fatigue life dependence on the mean stress is usually induced by the sensitivity of the direction of the load [13]. Chris et al. demonstrate that tensile mean stress, which sustained from the residual stress, can be approximated

✉ M. SreeArravind
sreearravind@sastra.ac.in

[1] School of Mechanical Engineering, SASTRA Deemed to be University, Thanjavur, Tamilnadu 613401, India

for the number of cycles to failure during LCF [14]. Tensile pre-strain affect the relaxation in the mean stress and can be observed only at strain amplitude more than 0.2% [15]. Surajit et al. illustrated stress-strain hysteresis loop aid to determine the cyclic yield stress, which directly correlates with the endurance limit [16]. In the stress-strain curve, the enclosed area, which represents dissipated plastic strain energy, influences fatigue life [17, 18]. Blochwitz et al. discussed plastic strain amplitude and orientation of grain influence crack initiation and propagation [19, 20]. Geometrically necessary dislocation density does not rely on dislocation pattern; rather, it depends on plastic stain amplitude [21]. Influence of the cyclic frequency fatigue life observed in BCC metals. From various observations conclude that fatigue strength gets enhanced with increase in cyclic frequency due to plastic straining acting on the crack nucleation region. Hence alloys were experiencing low plastic strain at other cyclic frequencies. In aluminum alloy, there is no significant influence observed [22]. Prolonged lifetime was observed in high loading frequency with enhanced endurance limit and depended on the testing environment [23].

The fatigue life of aluminum alloy is influenced by the embrittlement and localized oxidation, which contribute to crack length and the rate of crack propagation [24]. The clustering of particles at frequent intervals and mobile dislocation of strengthening precipitates in the matrix caused continuous deterioration in Al7055-T7751during low cycle fatigue [25]. Strain amplitude and a number of cycles decide dislocation pattern in 3003 Aluminum alloy [26, 27]. Eswara et al. concluded that every strain amplitude fractography for low cycle fatigue testing of Al-12Si-CuMgNi exhibited a combination of ductile fracture with micro dimples and brittle quasi cleavage fracture [28]. Ding et al. developed a model for predicting the crack growth and life during the low cycle fatigue test of aluminum matrix composite reinforced with short fiber [29]. Fatemi et al. employed the bilinear log-log model to represent the fatigue data of Aluminum alloys and found significant at long and short lives during the fatigue test [30]. Zheng et al. investigated the interaction between the low cycle and high cycle fatigue, found damages intense due to the plasticity in the crack tip and crack growth influenced by the LCF interaction persistently. They also proposed a model using the exponential law for the interaction damage with the account of loading parameters effect [31]. The initiation and propagation of fatigue crack induced in the region of un-recrystallized and recrystallized areas due to local stress concentration [32]. Micro additions like Ti, which acts as intermetallic precipitates, to induce a change in morphology in the aluminum alloy, thereby enhance the fatigue life of Al-7Si-1Cu-o.5 Mg alloy [33]. Nellessen et al. observed the deformation frequency of matrix and deformed Al single crystal misorientation influenced by the single crystal orientation. Al bi-crystals have some influence over the individual orientation of respective grains but instead induced neither the deformation band nor the local strain amplitude [34]. Haichun et al. obtained recurrent Orowan looping dislocation in incoherent precipitates leads to cyclic softening in over-aged AA6016 alloys cyclic hardening accompanied in under aged AA6016 due to precipitate growth and active precipitation during cyclic deformation [35].

In aluminum alloy, alloying element silicon influences the mechanical properties of the alloy. Natrayan et al. investigated the influence of silicon carbide in aluminum 2024 and found 3 wt% of SiC particulate enhanced the tribological properties and enhanced the thermal conductivity of the matrix [36]. Senthil et al. reported precipitates to enhance the mechanical behavior of the AA6061 matrix, which process through the encapsulating technique [37]. Moffat et al. observed high silicon content in aluminum pistol alloy, attributing to the fatigue crack propagation at elevated temperature by increasing the stress concentration factor [38]. The Authors in discussed the effect of alloying elements in the fatigue behavior of aluminum alloy ZL114A. At elevated temperature presence of Si, Fe, and Cu enhance the fatigue toughness [39]. Gonzalez et al. reported microstructural refining contributing to the fatigue behavior of heat treatable Al-Si alloy. The crack propagation depends on the porosity generated during the casting process [40]. Ali et al. observed the fatigue cracks initiated from the Si precipitate in Al-12Si (4047) alloy and in Al-5Si (4043) alloy crack initiated from the aluminum medium [41]. Literature focused on silicon in aluminum alloy, whereas the fatigue life improvement studies using the heat treatment in aluminum 6xxx series are not yet done. This particular work focused on analyzing the low cycle fatigue behavior of heat treated Al-Mg-Si alloy and the influence of silicon content in fatigue life at room temperature.

2 Materials and Methods

The Low cycle fatigue test is conducted for Al-Si-Mg aluminum alloy(AA6063) by using BISS Nano Plug n Play fatigue testing machine with the capacity of +25kN.The elemental composition of AA 6063 of the specimen was analyzed by the XPS method, and the percentage of elements is shown in Table 1.

In this alloy, the significant constituents Silicon (0.426%) and Magnesium (0.516%) of the total weight percent tend to disperse in the alloy to improve the mechanical property. AA 6063 alloy rods, with the individual dimensions of 15 mm as diameter and 100 mm long, were subjected to the solution heat treatment [42]. In the first phase, samples kept at 520 °C in the digital controlled muffle furnace with a maximum temperature range of 1200 °C for 2 h to attain the solution zing temperature. Following the solution heat treatment, one set of samples was quenched in the water medium at 27 °C. Then another set

Table 1 Elemental composition of AA 6063 extruded rod

Elements Wt%	Si	Fe	Cu	Mg	Mn	Zn	Ti	Cr	Al	Other elements
Standard	0.2–0.46	0.35 max	0.1 max	0.45–0.9	0.1 max	0.1 max	0.1 max	0.1 max	Balance	–
Tested	0.46	0.192	0.051	0.45	0.048	0.058	0.013	0.020	Remainder	0.050

of samples was air quenched at 27 °C. The samples attain the T42 temper designation through the above processes. To analyze the proper dispersion, un heat-treated, and heat-treated samples subjected to the X-ray diffraction analysis.

After the solution heat treatment, samples machined to the proper dimension, which was mentioned in Fig. 1a by adopting the ASTM E606 standard. Unheat-treated and heat-treated samples were subjected to the low cycle fatigue test with the total strain amplitude of 0.4% at the frequency of 0.3 Hz at room temperature in the fatigue machine, which is shown in Fig. 1b. The samples quenched in the water and air were compared with the results of a mean stress, stress-strain hysteresis loop, S N curve, and unheat-treated samples.

Fractography of the aluminum alloys taken using the scanning electron microscope (TESCAN, Japan) to illustrate the different fracture regions, crack propagation, and fatigue striation. In the following sections, the samples in the given format unheat-treated sample as WHT, heat-treated and air quenched as HTA, and heat-treated and water quenched as HTW.

3 Results and Discussion

Figure 2 illustrates the cyclic stress response for WHT, HTA, and HTW Al-Si-Mg aluminum alloy samples for TSA of 0.5%. WHT lasted upto 836 cycles until the failure; the stress amplitude starts with the range of 200 MPa and gradually decreased with the fluctuation. This decreasing trend indicates that the cyclic softening happened throughout life, the same kind of phenomenon described for under aged AA6063 at a strain amplitude of 0.5% [8].

This cyclic softening is happening because of the alteration of boundary orientation and minimalizing the defect density, stated with the previous fatigue property study of ultra-fine grained copper [43]. After the solution heat treatment, the HTA sample withstood about 1286 cycles, and interestingly the stress amplitude kept increasing up to 980 cycles, i.e., until the crack initiation. The same trend followed by the HTW sample, which lasted up to 708 cycles. The cyclic hardening effect in the LCF reported for heat treated Aluminum alloy samples8. In parallel, the air quenched sample sustained a higher number of cycles than water quenched because quenching of aluminum at a faster rate leads to increased distortion [44]. So the optimized quenching rate will be required for the aluminum alloys depend on the circumstance.

In low cycle fatigue, the mean stress plays a vital role in assessing the life of the material. The tensile and compressive mean stress showed in positive and negative regions. It defines the behaviour of the sample. Both phenomena may narrow the allowing stress [45]. Figure 3a showed the mean stress

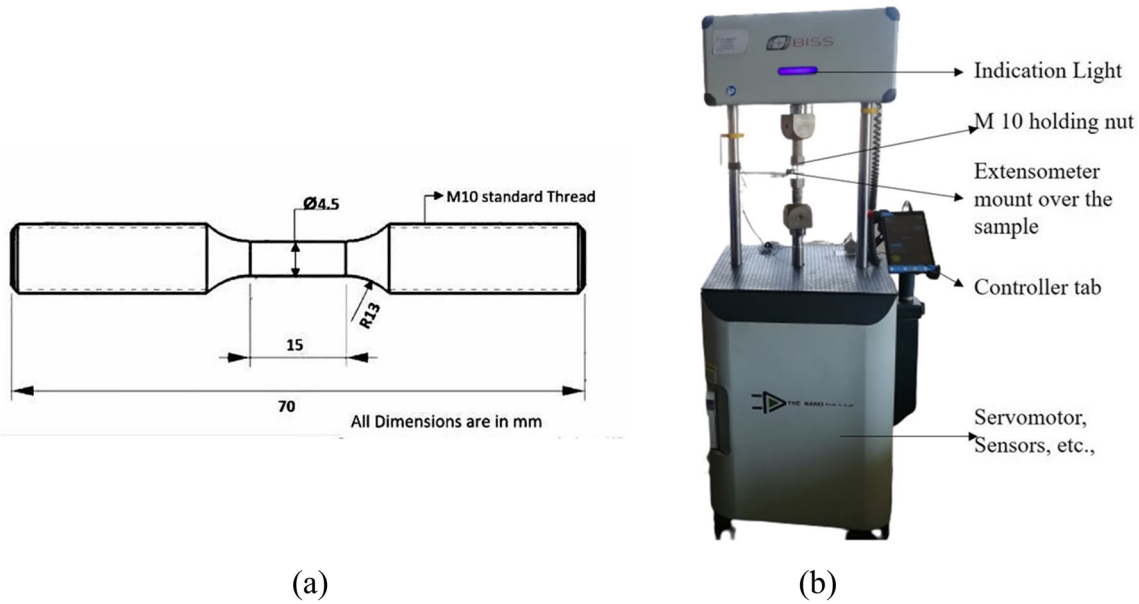

Fig. 1 **a** Dimension of the AA 6063 samples subjected to the low cycle fatigue test. **b** Low cycle fatigue machine

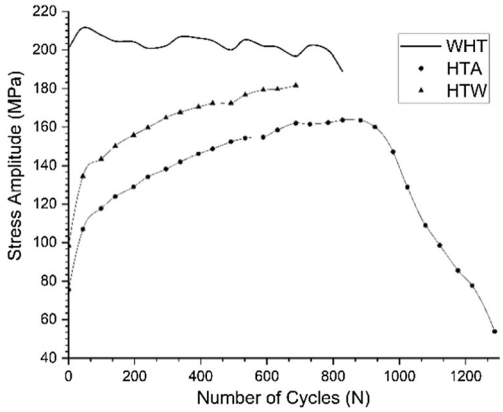

Fig. 2 Cyclic stress response of AA6063 samples with TSA of 0.4% at a cyclic frequency of 0.3 Hz

of the WHT sample starts with the mean stress (σ_m) of -5 MPa then it attained the positive value around $\sigma_m = 5$ MPa and sustain with the same value until the failure. Though the positive mean stress, due to the domination of the tensile part, cyclic softening happened until the failure. The phenomenon is reported on modified 9Cr-1Mo steel during the LCF test [46]. For the heat treated samples, HTA was shown in Fig. 3b and HTW, which is shown in Fig. 3c. The mean stress starts at $\sigma_m = -5$ MPa, and after the stabilization, the mean stress persisted zero, which caused the cyclic hardening [47]. Despite fatigue life, the quenching medium did not directly affect the mean stress, which can be observed through the graph plots (Fig. 3a-c). This cyclic hardening is due to the proper dispersion of the hardening elements after the solution heat treatment in the alloy [44].

Stress-strain hysteresis curve for the WHT, HTA, and HTW obtained similarly to FCC metals due to the deformation dominated by the slip dislocation [48]. Along with that, the unsymmetrical curvature shape of the loops indicated the differentiation in the tensile and compressive yield stress, which can be defined as the Bauschinger effect [49, 50]. The Basuchinger effect is confirmed by the increase in the yield strength in the plastic flow direction as the metal experiencing the plastic deformation [51].

Additionally, the non-linear elastic behavior of the WHT, HTA, and HTW in every phase was exhibited, as those were originated from the twining and reversible movement of dislocation [52]. The stress-strain curve for WHT sample under the total strain amplitude is given in Fig. 4a, in which the tensile yield stress value getting decreased with an increase in cycles. For cycle 1, stress value about $\sigma = 201$ MPa,

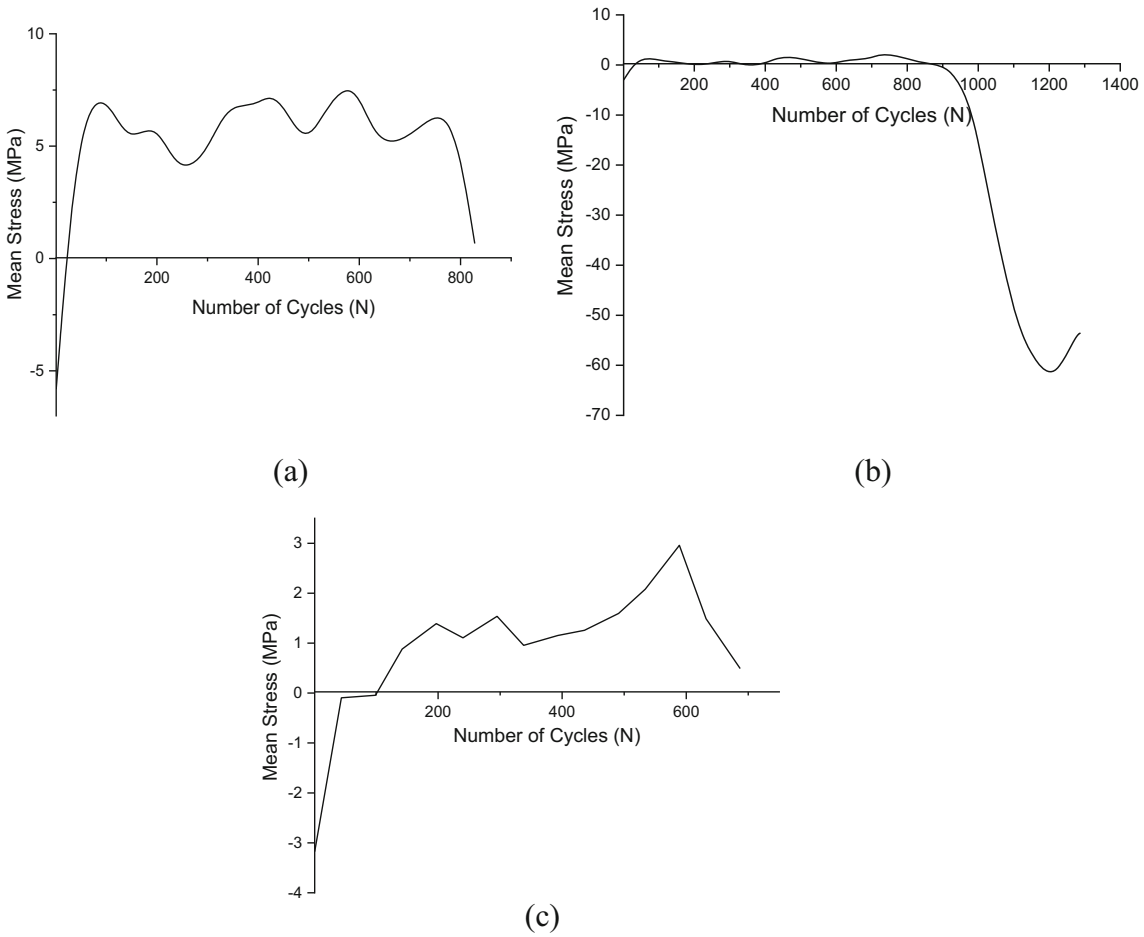

Fig. 3 Mean stress response of the AA 6063 with TSA of 0.4%. **a** Unheat-treated sample, **b** Air quenched sample, **c** Water quenched sample

190 MPa, and 185 MPa for cycle 400 and 600, respectively. For HTA, as shown in the Fig. 4b, due to the heat treatment and proper cooling rate, the stress value increased, i.e., for cycle 1, the stress is σ = 65 MPa, and for the cycle 500 and 600 stress value reached 145 MPa and 155 MPa respectively. When HTA specimen experiencing the tensile and compressive load cyclically, the plastic flow of the material influenced and lead to cyclic hardening. Thus the tensile yield stress of HTA sample increased with an increase in the cycle. This phenomenon is known as the Bauschinger effect [50]. Figure 4c, the initial cycle stress value as 75 MPa and stress at cycle 250 as 145 MPa, the HTW sample also exhibits cyclic hardening, this hardening is also found among the heat treated Mg alloy under the low cycle fatigue [53].

Plastic strain amplitude is also having a significant influence on fatigue life as it initiates internal cracks by influencing the grain [49]. Figure 5a-c shows the trend of plastic strain amplitude for WHT, HTA, and HTQ samples for 0.4% strain amplitude. For the unheat-treated, WHT sample, the plastic strain amplitude value started with $\Delta\varepsilon_p/2 = 0.062\%$, then maintained throughout the entire cycle, shown in Fig. 5a. HTA sample starts with the value of $\Delta\varepsilon_p/2 = 0.159\%$, as shown in fig. 5b. Furthermore, the HTW sample starts with the value of $\Delta\varepsilon_p/2 = 0.256\%$, as shown in Fig. 5c. Then both HTA and HTW samples reached $\Delta\varepsilon_p/2 = 0.05\%$ and remained constant throughout the entire life. The zone of transition occurred in the range of 30–60 cycles, afterward the slope decreased and sustained at nominal $\Delta\varepsilon_p/2$ value throughout the fatigue life. However, there is only less variation among the plastic strain amplitude trend among WHT, HTA, and HTW for 0.4% total strain amplitude because the $\Delta\varepsilon_p/2$ value relies on the change in total strain amplitude [54–56].

The variation in the elastic modulus is linked with the shape of the stress-strain loops, which reported by sommer

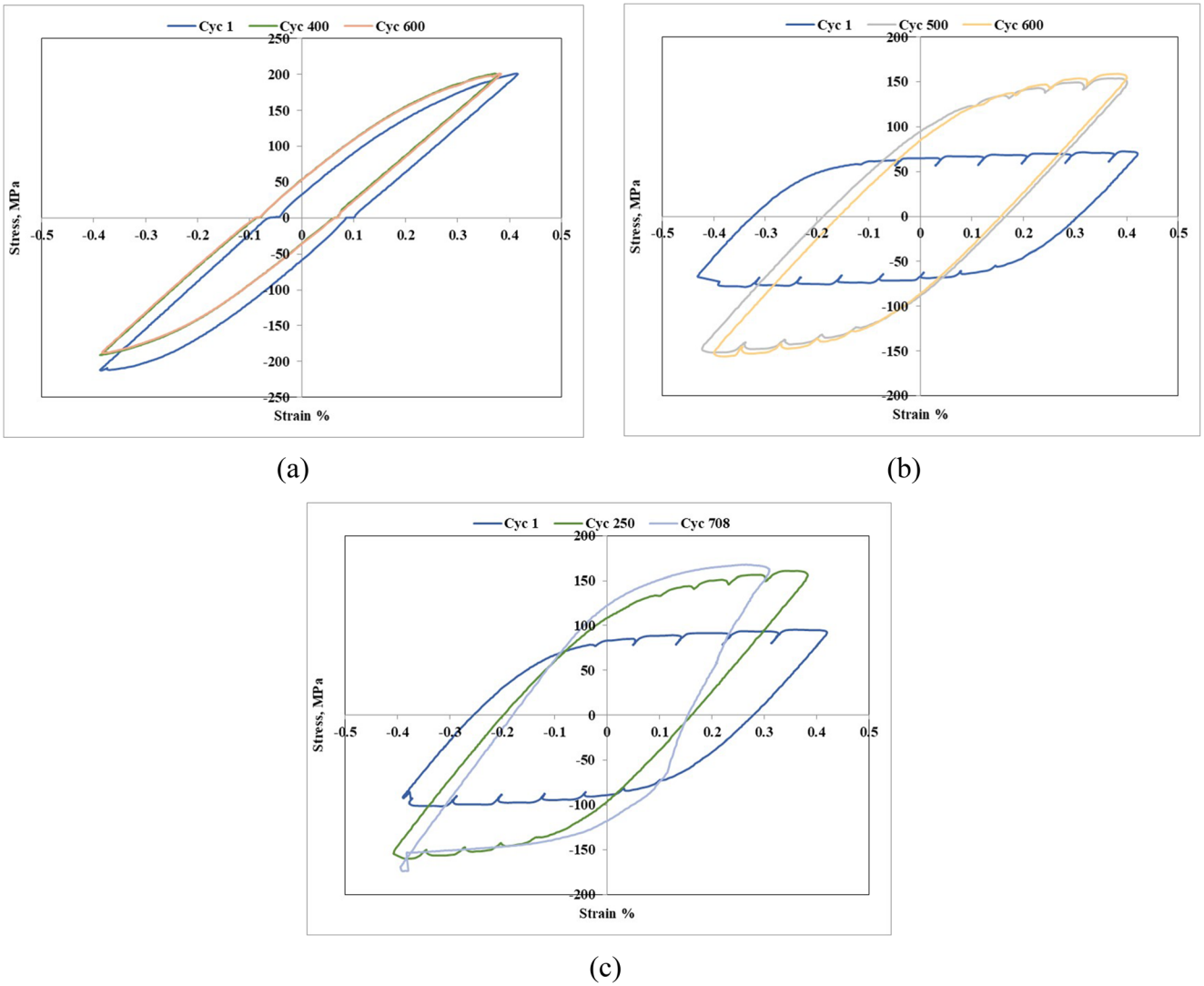

Fig. 4 Stress-strain hysteresis loop AA 6063 with TSA of 0.4%. **a** Unheat-treated sample, **b** Air quenched sample, **c** Water quenched sample

et al. for the roller bearing steel [57]. Figure 6a-c shows the unloading modulus of the samples for 0.4%TSA. The rigidity dominates the WHT sample because of its age hardening. Figure 6a shows that the unloading modulus of the material almost remains constant as the elastic strain retains it.

Thus the symmetries among the stress-strain loop can be obtained in Fig. 4a. Due to the cyclic hardening effect, the unloading modulus of heat treated samples kept changing. Figure 6b shows that the HTA sample started from 13 GPa, and due to an increase in rigidity, the modulus value kept in an increasing trend until the crack initiation. HTW also started with an unloading modulus of 20GPa, followed by HTA, shown in Fig. 6c. The effect of water quenching provides increased rigidity for the HTW sample due to the, so the value of unloading modulus reached unsymmetrical stress-strain curves24, which can be obtained from Fig. 4b and c.

The fractured surface of the AA 6063 samples was analyzed using the scanning electron microscope (SEM), shown in Figs. 7, 8 and 9. The macroscopic view of the fractured surface of the WHT sample is shown in Fig. 7a, in which the HTA sample exhibits both dimple rupture and cleavage fracture on the surface. The crack initiated from the weakest region of the specimen, which shown in Fig. 7b. Gall et al. [58] analyzed that casting defects may affect the fatigue life of the material by weakening a specific section.

Figure 7c secondary cracks obtained in union with the fatigue striation, which is observable in higher strain amplitude [59]. Figure 7d indicates the presence of two distinct fracture components, at the initial stage cleavage fracture, then transited to dimple rupture as the final fracture zone, the same observed for AA2017 alloy [60]. In Fig. 7e, micro voids are focused on the final fracture zone, which originated from the second phase particles [56].

The macroscopic view of the fractured surface of the air-quenched sample is shown in Fig. 8a, in which the HTA sample exhibits both dimple and tears ridges in the surface, so it accounted as a quasi-cleavage fracture [56]. Three

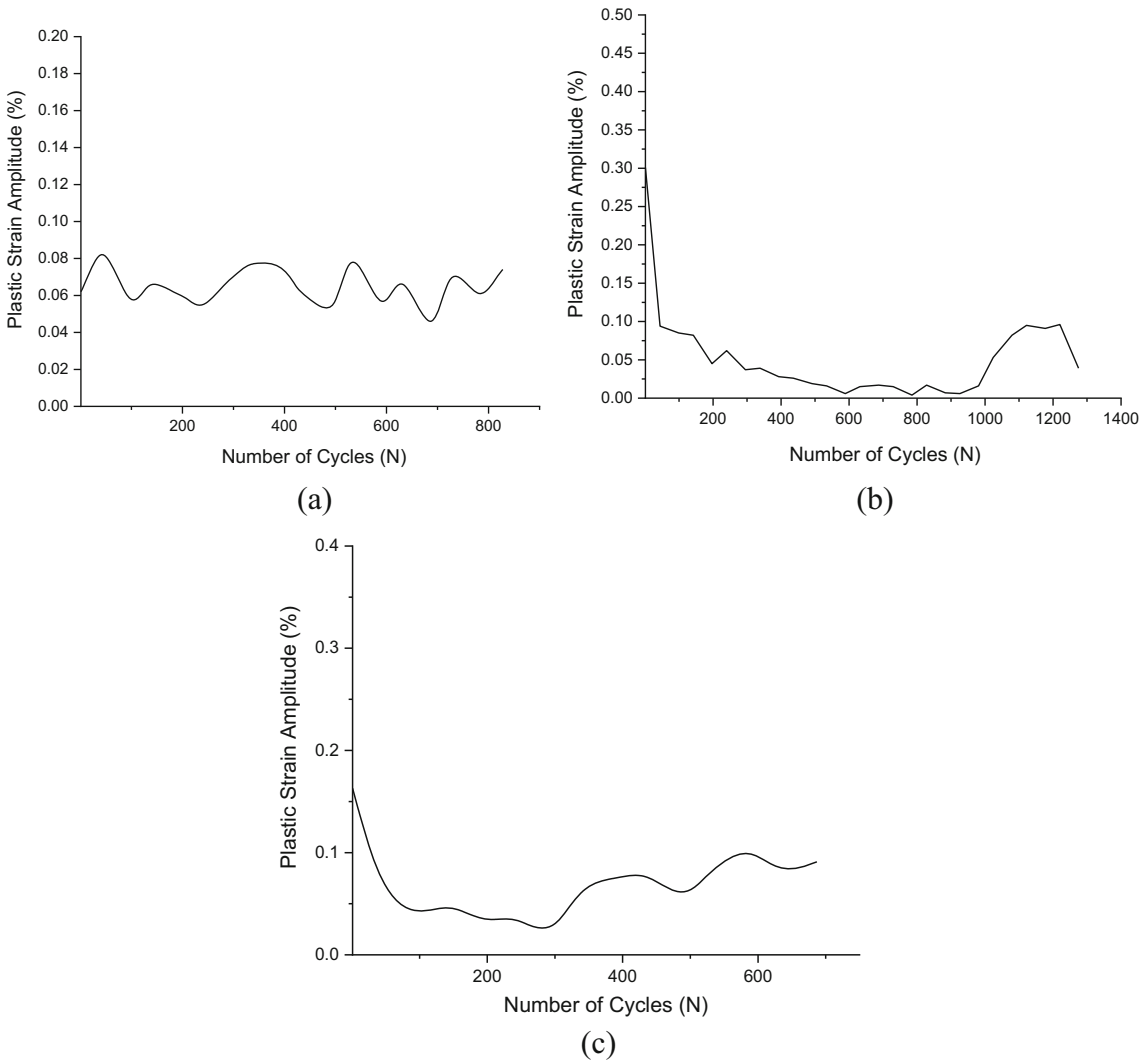

Fig. 5 The plastic strain amplitude response of AA6063 with TSA of 0.4%. **a** Unheat-treated sample, **b** Air quenched sample, **c** Water quenched sample

features of fatigue fracture, namely initiation of crack, crack growth, and ultimate fracture, can be observed in Fig. 8b.

Figure 8b-d depicts that the fractured surface constitutes planar and granular regions in the zone of crack propagation. These two distinct regions related to the altered grains and orientation changes in the grain boundary, which similarly observed for the fatigue fractured surface of AA2017 alloy [60]. Figure 8b shows beach marks on the surface, which indicates the steady propagation of the crack. From Fig. 8c, many striated plateaus in the planar fracture region can be traced for the direction of propagation of the crack. Figure 8d depicts the granular fracture region, which shows the transition phase of crack formation from the dimple rupture to quasi cleavage fracture. Figure 8e exposed the particular region from the planar fracture region to find the fatigue striation, which caused the ripple formation. This analysis implies that crack propagated in a ductile manner incorporated with the retardation and blunting of the propagated cracks [60].

The fractured surface of the water quenched sample is shown in Fig. 9a in which the HTW sample exhibits quasi-cleavage fracture since it exhibits both dimple rupture and cleavage around the periphery [56]. In some regions for the strain amplitude of 0.4%, the fracture depicts ductile transgranular regions in the granular fracture region, which is shown in Fig. 9b. In the same region obtained for AA7150, the transgranular regions are featureless, and cracks propagated along the boundaries, parallel to the direction of loading [61]. Water quenching of aluminum alloy induces hydrogen embrittlement [62], leading to early failure in fatigue testing [24].The precipitates were found in the granular fracture region, which resulted in the non-homogeneous deformation since it caused dislocation pileups, which showed in Fig. 9c. Srivatsan et al. stated that the contribution of the precipitates is negotiable, but in parallel, they influence the cyclic straining behavior [61]. Figure 9d planar fracture region with the fatigue striation which faces in the direction of crack propagation, reveals that the intermediated stage followed the

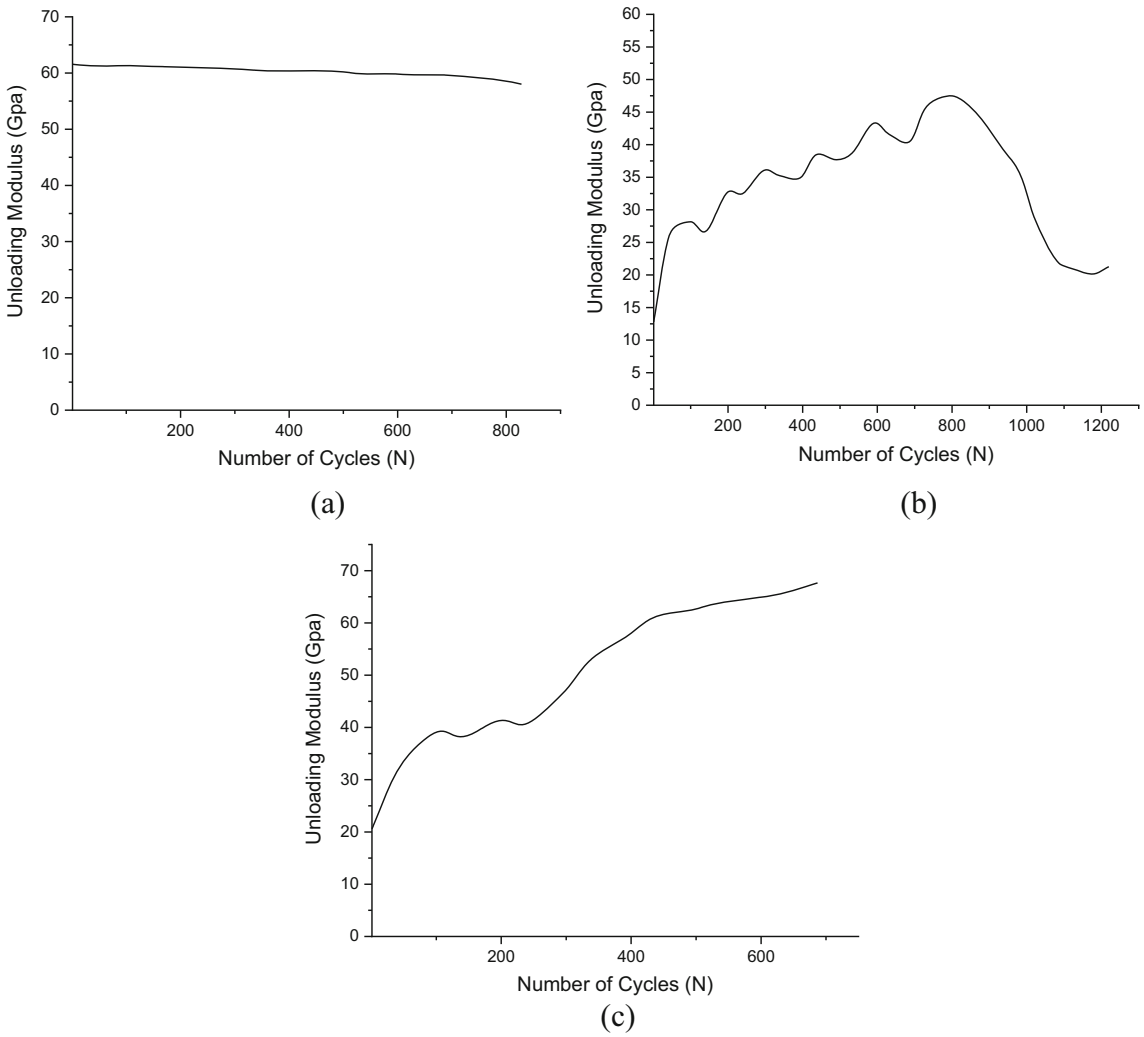

Fig. 6 Unloading Modulus response of AA 6063 with strain amplitude of 0.4%. **a** Unheat-treated sample, **b** Air quenched sample, **c** Water quenched sample

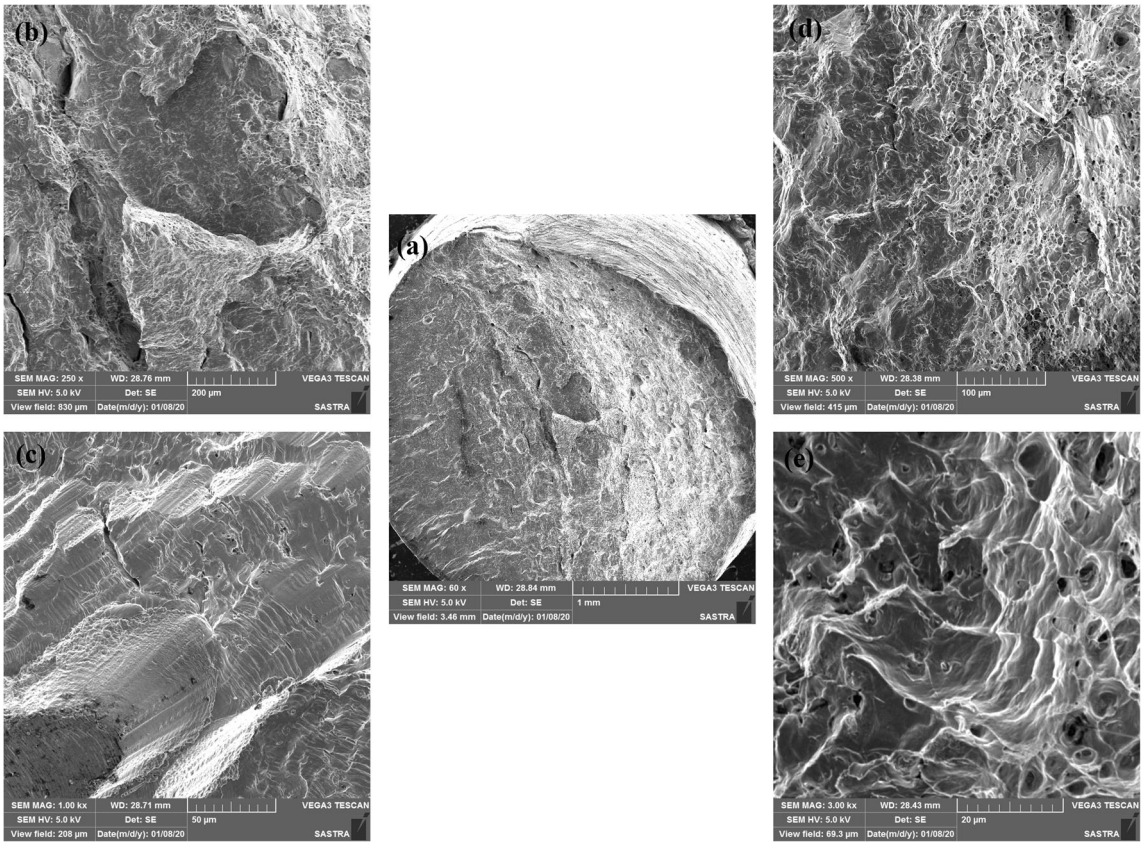

Fig. 7 Scanning electron microscopic image of unheat-treated sample fracture surface for the total strain amplitude of 0.4%

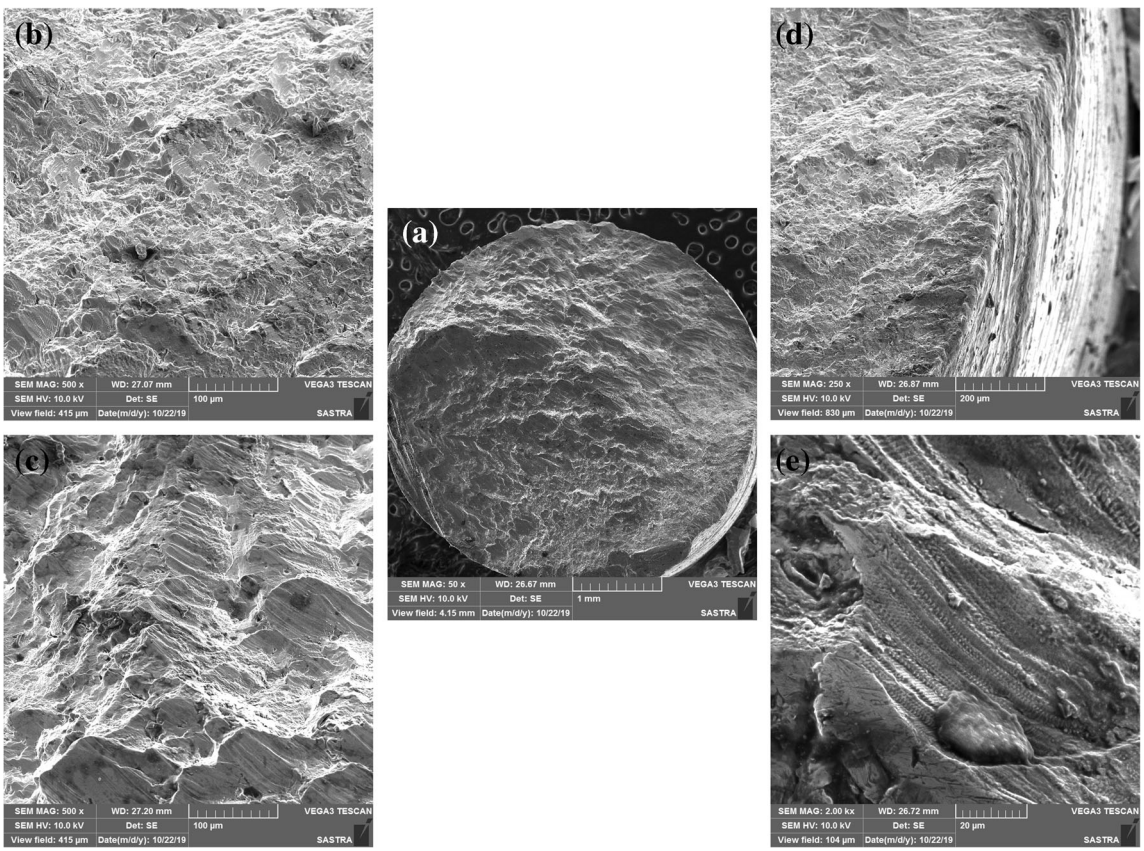

Fig. 8 Scanning electron microscopic image of air quenched sample fracture surface for TSA of 0.4%

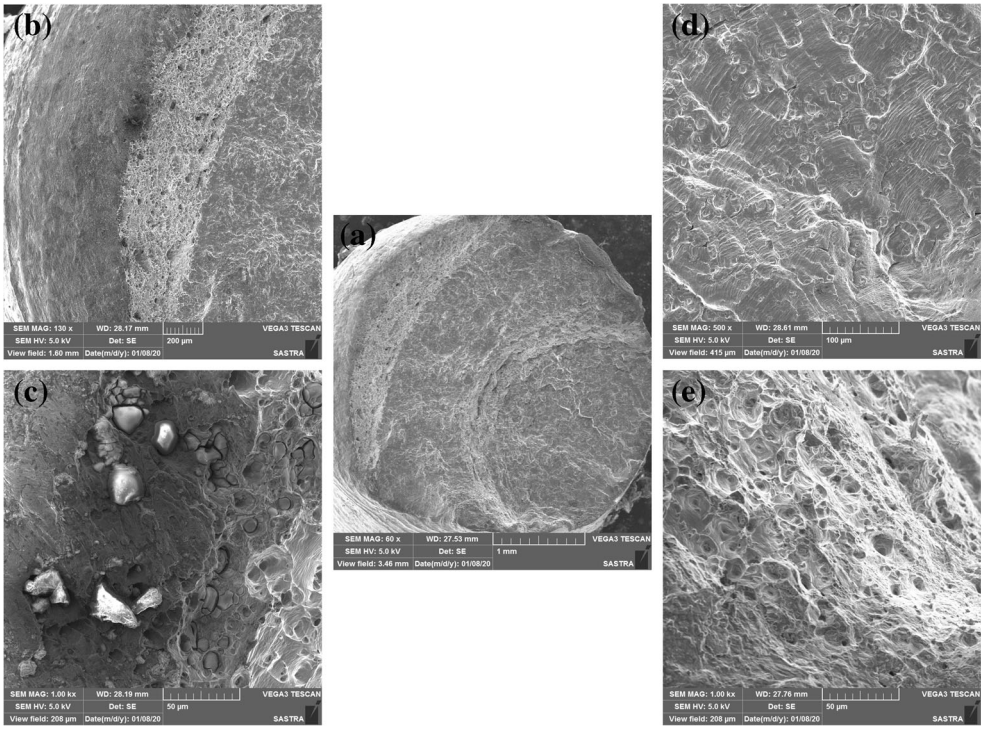

Fig. 9 Scanning electron microscopic image water quenched sample fracture surface for the total strain amplitude of 0.4%

brittle fracture, and Fig. 9e shows the micro void coalescence formed during the final stage of the failure. This phenomenon imitated at the precipitates, and then voids grow, and finally, the final failure happened [56].

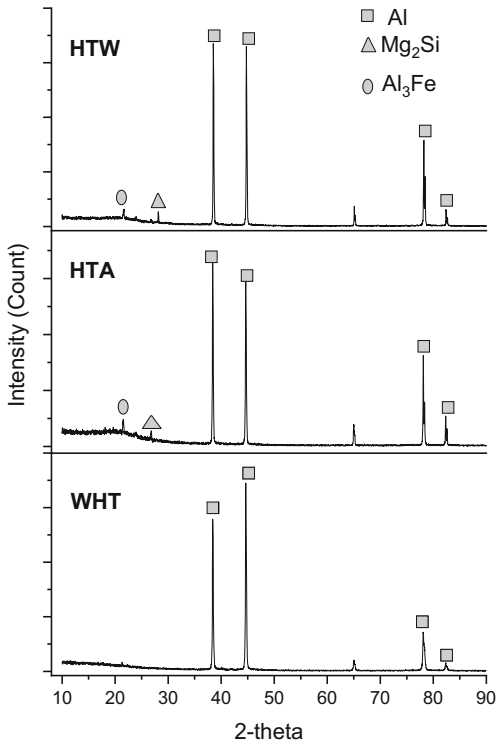

Fig. 10 XRD analysis of AA6063 samples before and after heat treatment

Dispersion of precipitates after the solution heat treatment has inveterate through the XRD analysis. The peaks for WHT, HTA, and HTW have shown in Fig. 10. The peaks detected for Mg_2Si and Al_3Fe in the heat-treated samples ensure the proper dispersion of precipitates during solution heat treatment [63]. The presence of precipitates Mg_2Si and Al_3Fe have influenced the fatigue behavior since precipitates act as a barrier for crack propagation in WHT and HTA samples [64]. So the fatigue life of HTA and WHT were higher than the water quenched sample.

4 Conclusion

Low cycle fatigue tests taken for the unheat treated and heat-treated Al-Si-Mg aluminum alloy, cyclic deformation characteristic such as unloading modulus along with the mode of fracture of the Al alloy were investigated, and the following inferences have drawn:

The fatigue life of heat-treated and air-quenched sample implies that fatigue life can be improved by the heat treatment and depends on the rate of cooling and quenching medium. The fatigue life of water quenched sample influenced by hydrogen embrittlement. From the test data, the fatigue life of AA6063 denoted in the order:

Air quenched AA 6063 sample > Unheat treated AA 6063 sample > Water quenched AA6063 sample.

Cyclic softening witnessed in the unheat-treated sample due to the twinning effect until the crack initiation and cycle hardening were observed in the heat-treated samples, which

confirms the Bauschinger effect. It is observed that the symmetrical property of the stress-strain curve and unloading modulus effects are directly related.

From the fractography, the direction of crack propagation identified through the striated plains and the retardation and blunting of the cracks confirms the cyclic hardening effect on the air-quenched sample. Precipitates were found in the heat-treated samples, as they influence the cyclic straining of the material. XRD analysis confirmed the proper dispersion of precipitates after the heat treatment.

Acknowledgments The authors thank SASTRA Deemed University for its financial assistance.

Availability of Data and Material The datasets analyzed during the current study are available from the corresponding author on reasonable request.

Author Contributions *Ramesh Kumar S:* Supervision, Methodology, Writing- Reviewing and Editing.

SreeArravind M: Investigation, Conceptualization, Software, Writing, Editing.

Funding This work is supported by the "Research and Modernization fund, SASTRA University" grant number R&M/0035/SoME-008/2015–16.

Compliance with Ethical Standards This article does not contain any studies with human participants or animals performed by any of the authors.

Conflict of Interest The authors declare that they have no conflict of interest.

Consent to Participate Not applicable.

Consent for Publication Not applicable.

References

1. Totten GE, Webster GM, Bates CE (2003) In: Totten GE and MacKenzie DS (eds) Handbook of aluminum. CRC Press, Florida
2. Croucher T (1982) Quenching of aluminum alloys: what this key step accomplishes. Heat Treat 14:20–21
3. Bates CE, Totten GE (1988) Procedure for quenching media selection to maximize tensile properties and to minimize distortion in aluminum-alloy parts. Heat Treat Met 4:89–98
4. Ridhwan J, Noor JA, Zakaria MS et al (2014) Effect of heat treatment on microstructure and mechanical properties of 6061 aluminum alloy. J Eng Technol 5:89–98
5. Ridhwan J, Hamzah E, Selamat MZ, Zulfattah Z, Hafidzal MHM (2013) Effect of aging treatment on the microstructures and hardness of Fe-Ni-Cr Superalloy. Int J Automot Mech Eng 8:1430–1441
6. Fragoudakis R, Karditsas S, Savaidis G, Michailidis N (2014) The effect of heat and surface treatment on the fatigue behaviour of 56SiCr7 spring steel. Procedia Eng 74:309–312
7. Zaiedah Nasir N, Mohd Daud MA, Selamat MZ, Rivai A, Dhar Malingam S (2014) The effect of heat treatment on fatigue and mechanical properties of 6061 Aluminium alloy. Appl Mech Mater 699:227–232
8. Nandy S, Sekhar AP, Das D, Hossain SJ, Ray KK (2016) Influence of dynamic precipitation during low cycle fatigue of under-aged AA6063 alloy. Trans Indian Inst Metals 69:319–324
9. Khalil O, Lang KH (2011) Influence of microstructure on the quasistatic and low cycle fatigue behaviour of an AA2618 aluminium alloy. Procedia Engineering 10:1339–1347. https://doi.org/10.1016/j.proeng.2011.04.223
10. Frodal BH, Christiansen E, Myhr OR, Hopperstad OS (2020) The role of quench rate on the plastic flow and fracture of three aluminium alloys with different grain structure and texture. Int J Eng Sci 150:103257
11. Liu S, Zhang M, Li Q, Zhu Q, Song H, Wu X, Cao L, Couper MJ (2020) Effect of quenching rate on strengthening behavior of an Al-Zn-mg-cu alloy during natural ageing. Mater Sci Eng A 793:139900
12. Kwofie S, Chandler HD (2001) Low cycle fatigue under tensile mean stresses where cyclic life extension occurs. Int J Fatigue 23:341–345
13. Winter L, Hockauf K, Winter S, Lampke T (2020) Equal-channel angular pressing influencing the mean stress sensitivity in the high cycle fatigue regime of the 6082 aluminum alloy. Mater Sci Eng A 795:140014
14. Bassindale C, Miller RE, Wang X (2020) Effect of single initial overload and mean load on the low-cycle fatigue life of normalized 300 M alloy steel. Int J Fatigue 130:105273
15. Branco R, Costa JD, Borrego LP, Wu SC, Long XY, Antunes FV (2020) Effect of tensile pre-strain on low-cycle fatigue behaviour of 7050-T6 aluminium alloy. Eng Fail Anal 114:104592
16. Paul SK (2020) Correlation between endurance limit and cyclic yield stress determined from low cycle fatigue test. Materialia 11:100695
17. Zhao Z, Chen X (2020) Effect of cyclic softening and stress relaxation on fatigue behavior of 2.25Cr1Mo0.25V steel under strain-controlled fatigue-creep interaction at 728 K. Int J Fatigue 140:105848
18. Wang R-Z, Zhang X-C, Tu S-T, Zhu SP, Zhang CC (2016) A modified strain energy density exhaustion model for creep–fatigue life prediction. Int J Fatigue 90:12–22
19. Senthil Kumar M et al (2019) Processing and characterization of AA2024/Al2O3/SiC reinforces hybrid composites using squeeze casting technique. Iran J Mater Sci Eng 16(2):55–67
20. Blochwitz C, Heinrich D, Frenzel R (1989) Microcrack propagation in fatigued F.c.c. monocrystals I: crack-depth distribution and propagation rate. Mater Sci Eng A 118:71–81
21. Kundu A, Field DP, Chandra Chakraborti P (2019) Influence of strain amplitude on the development of dislocation structure during cyclic plastic deformation of 304 LN austenitic stainless steel. Mater Sci Eng A 762:138090
22. Papakyriacou M, Mayer H, Pypen C, Plenk Jr H, Stanzl-Tschegg S (2001) Influence of loading frequency on high cycle fatique properties of b.c.c and h.c.p. metals. Mater Sci Eng A 308:143–152
23. Schneider N, Bödecker J, Berger C, Oechsner M (2016) Frequency effect and influence of testing technique on the fatigue behaviour of quenched and tempered steel and aluminium alloy. Int J Fatigue 93:224–231
24. Srivatsan TS (1988) Mechanisms of damage in high-temperature, low cycle fatigue of an aluminium alloy. Int J Fatigue 10:91–99
25. Srivatsan TS (1999) Mechanisms governing cyclic deformation and failure during elevated temperature fatigue of aluminum alloy 7055. Int J Fatigue 21:557–569
26. Fujii T, Watanabe C, Nomura Y et al (2001) Microstructural evolution during low cycle fatigue of a 3003 aluminum alloy. Mater Sci Eng A 319–321:592–596

27. Natrayan L, Senthil kumar M, Palanikumar K. (2018) Optimization of squeeze cast process parameters on mechanical properties of Al_2O_3/SiC reinforced hybrid metal matrix composites using taguchi technique. Mater Res Expr 5(6):066516
28. Eswara Prasad N, Vogt D, Bidlingmaier T, Wanner A, Arzt E (2000) High temperature, low cycle fatigue behaviour of an aluminium alloy (Al–12Si–CuMgNi). Mater Sci Eng A 276:283–287
29. Ding H-ZZ, Biermann H, Hartmann O (2003) Low cycle fatigue crack growth and life prediction of short-fibre reinforced aluminium matrix composites. Int J Fatigue 25:209–220
30. Fatemi A, Plaseied A, Khosrovaneh AK, Tanner D (2005) Application of bi-linear log–log S–N model to strain-controlled fatigue data of aluminum alloys and its effect on life predictions. Int J Fatigue 27:1040–1050
31. Zheng X, Engler-Pinto CCC, Su X et al (2013) Modeling of fatigue damage under superimposed high-cycle and low-cycle fatigue loading for a cast aluminum alloy. Mater Sci Eng A 560:792–801
32. Zeng L, Li Z, Che R, Shikama T, Yoshihara S, Aiura T, Noguchi H (2014) Mesoscopic analysis of fatigue strength property of a modified 2618 aluminum alloy. Int J Fatigue 59:215–223
33. Shaha SKK, Czerwinski F, Kasprzak W et al (2016) Effect of transition metals on energy absorption during strain-controlled fatigue of an aluminum alloy. Int J Fatigue 87:456–470
34. Nellessen J, Sandlöbes S, Raabe D (2016) Low cycle fatigue in aluminum single and bi-crystals: on the influence of crystal orientation. Mater Sci Eng A 668:166–179
35. Jiang H, Sandlöbes S, Gottstein G, Korte-Kerzel S (2017) On the effect of precipitates on the cyclic deformation behavior of an Al–mg–Si alloy. J Mater Res 32:4398–4410
36. Natrayan L, Kumar MS (2020) Influence of silicon carbide on tribological behaviour of AA2024/Al_2O_3/SiC/gr hybrid metal matrix squeeze cast composite using Taguchi technique. Mater Res Expr 6:1265f9
37. Natrayan L, Senthil Kumar M (2020) An integrated artificial neural network and Taguchi approach to optimize the squeeze cast process parameters of AA6061/Al_2O_3/SiC/gr hybrid composites prepared by novel encapsulation feeding technique. Mater Today Commun 25:101586
38. Moffat AJ, Barnes S, Mellor BG, Reed PAS (2005) The effect of silicon content on long crack fatigue behaviour of aluminium-silicon piston alloys at elevated temperature. Int J Fatigue 27(10–12):1564–1570
39. Dong XG, Zhou J, Jia YJ, Liu B (2012) Effect of alloying on high temperature fatigue performance of ZL114A (Al-7Si) alloy. Trans Nonferrous Metals Soc China 22:661–667
40. González JA, Talamantes-Silva J, Valtierra S, Colás R (2017) Fatigue in a heat treatable high silicon containing aluminium alloy. J Phys IOP Conf Ser 843:12027
41. Shomran AT, Hussein EK, Shomran HT, Gaaz TS, Takriff MS, Kadhum AAH, al-Amiery AA (2020) Investigation of adding silicon on fatigue properties of aluminum based alloys. Silicon. https://doi.org/10.1007/s12633-020-00500-7
42. Standard Practice for Heat Treatment of Aluminum-Alloy Castings from All Processes, ASTM International B917/B917M-12. ASTM Book of Standards, 2012. https://doi.org/10.1520/B0917
43. Agnew S, Weertman J (1998) Cyclic softening of ultrafine grain copper. Mater Sci Eng A 244:145–153
44. Kavalco PM, Canale LCF, Totten GE (2009) Quenching fundamentals; quenching of aluminum alloys: cooling rate, strength, and Intergranular corrosion. http://web.archive.org/web/20200828034324/https://www.asminternational.org/c/portal/pdf/download?articleId=HTP00907P25&groupId=10192. Accessed 2 Aug 2019
45. Karakaş Ö, Szusta J (2016) Monotonic and low cycle fatigue behaviour of 2024-T3 aluminium alloy between room temperature and 300 °C for designing VAWT components. Fatigue Fract Eng Mater Struct 39:95–109
46. Zhou H, He Y, Zhang H, Cen Y (2013) Influence of dynamic strain aging pre-treatment on the low-cycle fatigue behavior of modified 9Cr-1Mo steel. Int J Fatigue 47:83–89
47. Yin SY, Chen LJ, Wang X (2011) Influence of heat treatment on low-cycle fatigue behavior of AZ61 magnesium alloy. Adv Mater Res 287–290:883–887
48. Suresh S (1988) Fatigue of materials2nd edn. Cambridge University Press, Cambridge
49. Begum S, Chen DL, Xu S, Luo AA (2009) Low cycle fatigue properties of an extruded AZ31 magnesium alloy. Int J Fatigue 31:726–735
50. Begum S, Chen DL, Xu S, Luo AA (2008) Strain-controlled low-cycle fatigue properties of a newly developed extruded magnesium alloy. Metall Mater Trans A 39:3014–3026
51. Jordon JB, Horstemeyer MF, Solanki K, Xue Y (2007) Damage and stress state influence on the Bauschinger effect in aluminum alloys. Mech Mater 39:920–931
52. Cáceres C, Sumitomo T, Veidt M (2003) Pseudoelastic behaviour of cast magnesium AZ91 alloy under cyclic loading–unloading. Acta Mater 51:6211–6218
53. Wang Q, Liu W, Wu G, Chen X, Zhang H (2017) Influence of heat treatment on cyclic deformation and low-cycle fatigue behavior of sand-cast mg–10Gd–3Y–0.5Zr magnesium alloy. J Mater Res 32:2179–2187
54. Noster U, Scholtes B (2003) Isothermal strain-controlled quasi-static and cyclic deformation behavior of magnesium wrought alloy AZ31. Zeitschrift fuer Met Res Adv Tech 94:559–563
55. Hasegawa S, Tsuchida Y, Yano H, Matsui M (2007) Evaluation of low cycle fatigue life in AZ31 magnesium alloy. Int J Fatigue 29:1839–1845
56. Dieter GE (1988) Mechanical metallurgy. McGraw-Hill, New York
57. Sommer C, Christ H-J, Mughrabi H (1991) Non-linear elastic behaviour of the roller bearing steel SAE 52100 during cyclic loading. Acta Metall Mater 39:1177–1187
58. McDowell D, Gall K, Horstemeyer M, Fan J (2003) Microstructure-based fatigue modeling of cast A356-T6 alloy. Eng Fract Mech 70:49–80
59. Mirza FA, Chen DL, Li DJ, Zeng XQ (2013) Low cycle fatigue of a rare-earth containing extruded magnesium alloy. Mater Sci Eng A 575:65–73
60. Hemmouche L, Fares C, Belouchrani MA (2013) Influence of heat treatments and anodization on fatigue life of 2017A alloy. Eng Fail Anal 35:554–561. https://doi.org/10.1016/j.engfailanal.2013.05.003
61. Srivatsan TS (1991) The low-cycle fatigue and cyclic fracture behaviour of 7150 aluminium alloy. Int J Fatigue 13:313–321. https://doi.org/10.1016/0142-1123(91)90358-6
62. Kumar S, Namboodhiri TKG (2011) Precipitation hardening and hydrogen embrittlement of aluminum alloy AA7020. Bull Mater Sci 34:311–321
63. Leszczyńska-Madej B, Richert M, Wąsik A, Szafron A (2017) Analysis of the microstructure and selected properties of the Aluminium alloys used in automotive air-conditioning systems. Metals (Basel) 8:10
64. Nowotnik GM, Sieniawski J, Wierzbińska M et al (2007) Intermetallic phase particles in 6082 aluminium alloy. Arch Mater Sci Eng 28:69–76